

Complete excitation spectrum of charge-density waves: Optical experiments on $K_{0.3}MoO_3$

L. Degiorgi, B. Alavi, G. Mihály,* and G. Grüner

*Department of Physics and Solid State Science Center, University of California at Los Angeles,
Los Angeles, California 90024*

(Received 11 March 1991)

Frequency-dependent conductivity measurements are reported in the charge-density-wave state of $K_{0.3}MoO_3$ and $K_{0.3}Mo_{1-x}W_xO_3$ alloys in the radio-frequency, microwave, millimeter-wave, and infrared spectral range. We identify several distinct features associated with the electrodynamics of the ground state. The dynamics of internal deformations of the collective mode, appearing at radio frequencies, together with the pinned-mode resonance at millimeter-wave frequencies are analyzed in detail and we evaluate the parameters that characterize these modes. We also identify a resonance in the far-infrared spectral range and suggest that it is due to bound charge-density-wave states. We account for the phonon spectra in terms of a phase-phonon description and also analyze the optical response due to single-particle excitations across the gap.

I. INTRODUCTION

Many different aspects of the electrodynamics of the charge-density-wave (CDW) ground state have been explored in recent years by conducting frequency-dependent transport measurements on various model compounds. In contrast to superconductors, where all the relevant excitations are above the single-particle gap (except at temperatures close to the immediate vicinity of T_c), in the CDW ground state several features are observed in the optical spectrum.¹ Single-particle excitations, with the onset frequency 2Δ , where Δ is the CDW gap, are clearly recovered in various compounds. Unlike in the case of superconductors, nearly all the spectral weight is associated with these excitations, and the appearance of single-particle transitions is not dependent on whether the clean or dirty limit applies to the materials in question. The collective mode excitation is shifted from zero to a finite frequency ω_0 (called the pinning frequency) because of the interaction of the collective mode with lattice imperfections. The dynamic of the state is characterized by a large effective mass m^* , and, consequently, the spectral weight of the collective mode is small, of the order of m_b/m^* , where m_b is the band mass. Internal excitations of the condensate lead to a low-frequency contribution to $\sigma(\omega)$, in the spectral range well below ω_0 , and this contribution also depends strongly on screening effects due to the uncondensed electrons. The optical response due to phonons is also influenced by CDW formation through the electron-phonon coupling. Finally, amplitude excitations, which are purely Raman active in a translationally invariant ground state, can, in principle, be optically active due to Brillouin zone folding and impurity effects.

Several aspects of the above-mentioned excitations have been discussed in the literature, and several important features of the optical spectrum are well understood.¹ Others have not been discussed or compared

with the various models in detail. In this paper we summarize our optical experiments on the model compound $K_{0.3}MoO_3$ and its alloys. $K_{0.3}MoO_3$ is an anisotropic metal with a chainlike crystal structure. The material undergoes a metal-insulator transition at $T=180$ K, and structural studies clearly establish the development of an incommensurate CDW state, which occurs along the chain direction.¹ The experiments have been conducted over an extremely broad spectral range, involving audio-frequency, radio-frequency, microwave, millimeter-wave, and optical measurements. Several of the features we have obtained rely heavily on the combination of experimental data taken in the different frequency ranges. In addition, we also demonstrate that such a combination is essential for a reliable evaluation of the parameters that characterize the various excitations, and make a detailed comparison with the theories of charge-density-wave dynamics.

In Sec. II we summarize our experimental methods and results. A discussion of the relevant features of the complete optical spectrum is presented in Sec. III, while our conclusions are summarized in Sec. IV. Some of our experimental results have been reported earlier.²⁻⁴

II. EXPERIMENTAL METHODS AND RESULTS

We have used a variety of experimental methods in order to evaluate the complex conductivity $\sigma = \sigma_1 + i\sigma_2$ (or $\sigma = \sigma' + i\sigma''$) over a broad spectral range. The fundamental parameters σ_1 and σ_2 are related to various measured quantities. In some cases, however, we have to rely on universal relations between the two components of the optical conductivity in order to evaluate σ_1 and σ_2 . In all cases, the applied electric field and the resulting currents flow along the chain direction. The excitation amplitude associated with the various methods is always small, and linear response theory applies. We will use this aspect of our experiments extensively later, when the electro-dynamics is evaluated over a broad spectral range.

At low frequencies (10^{-3} – 10^6 Hz) the complex conductivity was derived by Laplace transforming the time dependence of the charging current.⁵ For experiments above 10 MHz the sample was mounted at the end of a 50- Ω wave guide, and the impedance was monitored as a function of frequency in a compensated bridge circuit using a Hewlett-Packard HP-8754A network analyzer. The intermediate-frequency range (i.e., between 1 and 10 MHz) was covered by conventional ac impedance measurement, where the in-phase and out-of-phase voltage responses were measured under constant frequency current driving. This provides an overlap between the low- and high-frequency limits. The experiments were performed in a two-probe configuration of $K_{0.3}MoO_3$ single crystals with lengths ranging from 750 μm to 14 mm and cross sections between 0.0004 and 1.1 mm^2 . Samples of different geometries gave identical results for the dielectric constant, within the experimental error of size determination. The dielectric response is thus clearly not due to the contacts, but reflects the properties of the specimen.

Bridge and resonant cavity configurations have been employed to evaluate the complex conductivity in the microwave and millimeter-wave spectral range, techniques, which have been described in Ref. 6.

The optical reflectivity of large single crystals were measured in an extended photon energy range from 10^5 down to 10 cm^{-1} using linearly polarized light, in a temperature range between 5 and 300 K. In order to cover the whole energy range, we made use of four spectrometers. In the far-infrared (FIR) part of the spectrum we have used a Bruker Fourier spectrometer with triglycine sulfate detectors down to 25 cm^{-1} and with a liquid-helium-cooled germanium bolometer from 100 to 10 cm^{-1} . The incident light was alternately polarized both parallel and perpendicular to the metallic b -axis direction. After performing the reflectivity measurements, the crystals were covered with about a 1000- \AA thick layer of gold to calibrate the effects of residual surface roughness.

The crystals used in this study have been grown by electrolytic reduction of a molten mixture of K_2MoO_4 and MoO_3 . The successful crystallization is dependent upon the reduction temperature and the moderation of K_2MoO_4 to MoO_3 . In order to prepare $K_{0.3}MoO_3$, we used a simple electrolytic cell and employed platinum electrodes. Calcinated K_2MoO_4 was ground with MoO_3 in a ratio of 1:3.35–3.5. The mixture was melted around 550–600 $^\circ\text{C}$, and subsequently poured into a Pyrex watch glass. This mixture was then ground coarsely and placed in the electrolytic cell, where it was remelted around 560 $^\circ\text{C}$. The electrolysis is usually performed at low current densities (10–20 mA). The crystals, formed on the cathode, are harvested periodically. The tungsten (W) -doped crystals are grown with the same technique. Doping with WO_3 yields crystals in which the W concentration varies widely, but doping with K_2WO_4 results in a fairly uniform impurity distribution, as confirmed by electron microprobe analysis.

The conductivity, measured at dc and also at various micrometer- and millimeter-wave frequencies, is displayed in Fig. 1. We have found that at room temper-

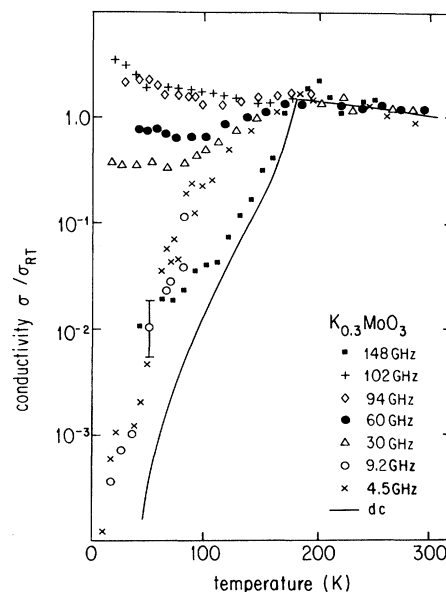


FIG. 1. Temperature dependence of the conductivity of $K_{0.3}MoO_3$ at dc and at various frequencies in the microwave and millimeter-frequency ranges.

ature the conductivity measured at different frequencies is, within experimental error (approximately 30%), the same as the dc value, as expected for a metal with a relaxation time in the optical spectral range ($10^2 < \tau^{-1} < 10^3\text{ cm}^{-1}$). Consequently, we have normalized all data to the dc conductivity of $\sigma_{dc} = 2000\text{ }\Omega^{-1}\text{cm}^{-1}$ for $K_{0.3}MoO_3$ at 300 K. In the metallic state the conductivity has the same temperature dependence at all frequencies. However, below $T = 180\text{ K}$, the charge-density wave develops, and σ is strongly frequency dependent. The data displayed in the figure suggests a strong resonance centered at 100 GHz (3.33 cm^{-1}), which becomes progressively sharper as the temperature is reduced.

The data in Fig. 1 has been combined with experimental results conducted at lower frequencies,^{7–9} and in Fig. 2 the CDW conductivity,

$$\sigma'_{CDW}(\omega) = \sigma'_{total}(\omega) - \sigma_{dc},$$

is plotted at different temperatures. The high-frequency peak (at 100 GHz) corresponds to the microwave and millimeter-wave results shown in Fig. 1. In the intermediate-frequency range, we include the data of Hall, Sherwin, and Zettl⁷ and of Reagor and Mozurkewich.⁸ The curves overlap within a factor of 2 at $T = 77\text{ K}$ (the common temperature of their experiments), and agree well with the data of Cava *et al.*,⁹ which are also shown in the figure.

The reflectivity spectrum for the pure $K_{0.3}MoO_3$ and for the alloy $K_{0.3}Mo_{1-x}W_xO_3$ with $x = 0.015$ is shown in Figs. 3(a) and 3(b). For both compounds we can divide the investigated energy spectral range in three parts, namely, the high-frequency (UV energy range) down to the middle IR (i.e., between 10^3 and 10^5 cm^{-1}), the far-infrared (FIR) (i.e., between 10 and 10^3 cm^{-1}), and the

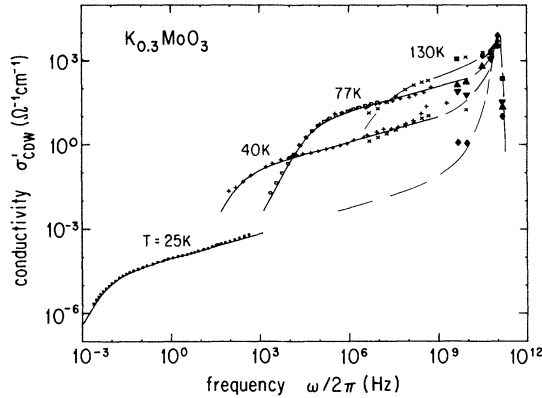


FIG. 2. Frequency dependence of the CDW conductivity at various temperatures. In the intermediate-frequency range, data of Ref. 7 (+), Ref. 8 (\times), and Ref. 9 (\square) are plotted. The low-frequency data are obtained by Laplace transformation from real-time experiments (Ref. 5). The solid line corresponds to Eq. (4), with $1-n=0.7$, and with τ_n following the temperature dependence of the normal resistivity. The dashed lines are guides to the eye.

low-frequency spectral range investigated with microwave and millimeter-wave techniques (i.e., between 10^{-2} and 10 cm^{-1}). In the higher part of the optical spectrum $R(\omega)$ is characterized by the interband transitions (which typically involve the d states of Mo and the p and s states of O of the octahedral MoO_6 units) and in the visible energy range by the sharp absorption edge ascribed to the Peierls gap. The FIR part of $R(\omega)$ shows

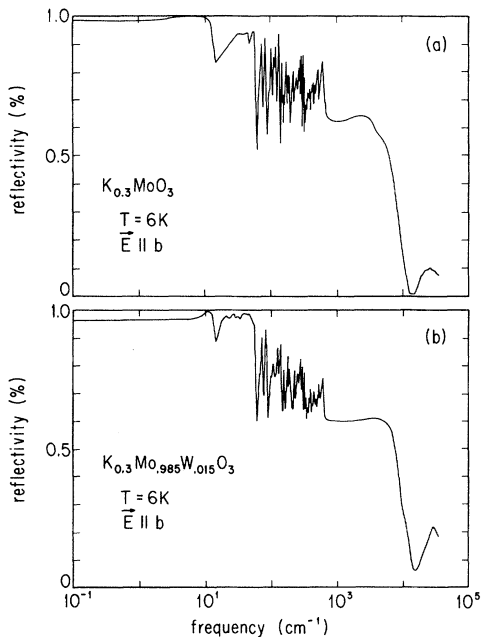


FIG. 3. Reflectivity $R(\omega)$ at 6 K of $\text{K}_{0.3}\text{MoO}_3$ (a) and $\text{K}_{0.3}\text{Mo}_{1-x}\text{W}_x\text{O}_3$ ($x=0.015$) (b), for polarization parallel to the conducting chains.

many sharp lines, which will be extensively discussed later, and a giant absorption at around 40 cm^{-1} . Finally, in the low-frequency energy range (of the order of a few wave numbers) another resonance clearly appears as evaluated from the direct measurement of σ_1 and σ_2 (see below).

III. DISCUSSION

In contrast with conventional semiconductors, where only phonon lines appear in the spectral range below the single-particle gap, in the CDW state we observe a variety of phenomena, which lead to optical features in an extremely wide spectral range and which we now discuss in detail. In the radio-frequency spectral range, the strongly temperature-dependent broad tail clearly displayed in Fig. 2 is related to the internal deformations of the phason mode.² The resonance at $\omega_{01}=3.33$ cm^{-1} (100 GHz), the so-called pinning frequency, is due to the oscillatory response of the collective mode. The resonance, which occurs at $\omega_{02}=40$ cm^{-1} in $\text{K}_{0.3}\text{MoO}_3$, has not yet been identified, although several frequencies above ω_{01} and below Δ/\hbar may be associated with the various excitations of the charge-density-wave condensate: amplitude mode, longitudinal-optical phason, zone-boundary acoustic phason, and/or resonant mode due to nonhomogeneities such as impurities or defect vacancies. We have argued earlier that these cannot account for this resonance in $\text{K}_{0.3}\text{MoO}_3$ and in $(\text{TaSe}_4)_2\text{I}$,³ and therefore experiments on other materials would be required to establish the origin of this mode. The phonon lines, which are observed in the far-infrared spectral range, are also influenced by the observation of the charge-density-wave mode.¹⁰ Finally, the rise of σ_1 in the infrared spectral range is due to single-particle excitations across the gap. In this section we discuss the various features of the optical spectrum in detail, and compare them with theories of charge-density-wave dynamics.

A. Low-frequency collective mode dynamics

Figure 2 indicates that the spectrum of the charge-density-wave excitations extends over a broad spectral range with considerable dynamics below the GHz frequencies. However, a different representation of the same experimental data reveals that the resonance around 100 GHz dominates the response. In Fig. 4 $\omega\sigma'_{\text{CDW}}(\omega)$ is plotted on a logarithmic frequency scale. In this plot the spectrum contains only one narrow peak at ω_0 , and no sign of any excitation is apparent at lower frequencies. In this representation the area below the curves corresponds to the oscillator strength:

$$A = \frac{2}{\pi} \int \omega \sigma_1(\omega) d(\ln \omega) = \frac{2}{\pi} \int \sigma_1(\omega) d\omega. \quad (1)$$

It is evident that most of the oscillator strength, associated with the collective response of the condensate, is due to the high-frequency resonance. The inset of Fig. 4 demonstrates that A is conserved as a function of the temperature, the relatively broad response at 130 K con-

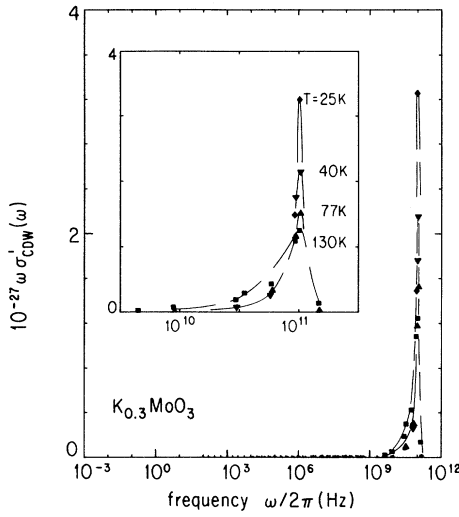


FIG. 4. $\omega\sigma'_{\text{CDW}}(\omega)$ vs frequency showing a single peak at ω_0 . The inset shows the resonance around 100 GHz. The dashed lines are guides to the eye. (The symbols are the same as in Fig. 2.)

tinuously transforms to a narrow, large amplitude peak. In a simple model, which assumes that the response is that of a harmonic oscillator, the oscillator strength is related to the effective mass of the condensate, $A = n_e e^2 / m^*$, and corresponds to a mass enhancement⁴ of $m/m_b \simeq 300$ (n_e is the number of electrons condensed into the CDW and m_b is the band mass), this value will be discussed later.

The low-frequency part of the spectrum becomes evident in a different representation. Figure 5 shows the imaginary part of the dielectric function, $\epsilon_2(\omega) = 4\pi\sigma_1(\omega)/\omega$, on a logarithmic frequency scale, which emphasizes the low-frequency excitations. The characteristic frequency of ϵ_2 dramatically drops with decreasing temperature and the peak shifts from the MHz range to 10^{-2} MHz in the temperature range investigated. According to the Kramers-Kronig relation, the integrated area associated with ϵ_2 corresponds to the static dielectric constant [$\epsilon_1(\omega=0) \gg 1$]:

$$\epsilon_1(\omega=0) = \frac{2}{\pi} \int \frac{\epsilon_2(\omega)}{\omega} d\omega = \frac{2}{\pi} \int \epsilon_2(\omega) d(\ln\omega). \quad (2)$$

Curves shown in Fig. 5 reflect a progressively increasing static dielectric constant. At $T=77$ K, $\epsilon_1(\omega=0) = 1.1 \times 10^7$; at 40 K it reaches a value of 4.3×10^7 , and the integrated area at 25 K would correspond to $\epsilon_1(\omega=0) > 10^8$. As the peak of ϵ_2 shifts below the experimentally reasonable time scale, the true static value of ϵ_1 cannot be measured.¹¹ Figure 5 indicates that an experimental cutoff on the order of 10 s only allows the measurement of about 30% of the static value at $T=25$ K. It was found that $\epsilon_1(\omega \rightarrow 0)$ continuously increases with decreasing temperature, and it does not saturate¹² or drop¹³ at low temperatures.

The low-frequency behavior has been examined by

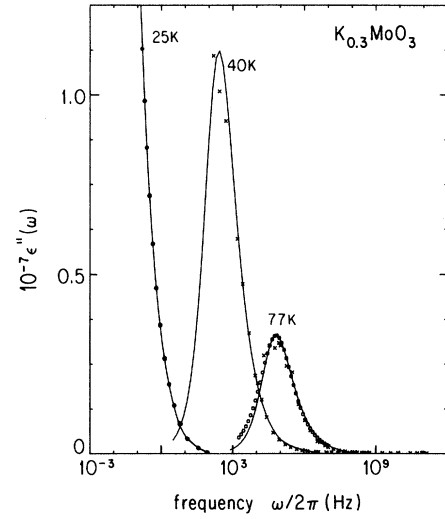


FIG. 5. Imaginary part of the dielectric constant vs frequency. The integrated area gives the static dielectric constant. The solid lines correspond to Eq. (4) with the same parameters as in Fig. 2. (The symbols are the same as in Fig. 2.)

different groups,^{5,9} and the strong temperature dependence of the dielectric response has been recognized. The smeared out peak in $\epsilon_2(\omega)$, as well as the low-frequency tail in the spectrum, are usually analyzed in terms of phenomenological expressions derived originally for random systems. One phenomenological description of the results, which has been proposed,⁹ uses the generalized Debye formula of Havriliak and Negami¹⁴

$$\epsilon(\omega) = \epsilon_\infty + (\epsilon_0 - \epsilon_\infty) \frac{1}{[1 + (i\omega\tau_m)^{1-\alpha}]^\beta}, \quad (3)$$

and introduce a formal distribution function of the relaxation times around the mean value τ_m . [Here ϵ_0 and ϵ_∞ are the static and the $\omega \rightarrow \infty$ dielectric constant, α and β are weakly temperature-dependent parameters with $(1-\alpha)\beta = 0.7$.] The average relaxation frequency, $\omega_m = 1/\tau_m$, was found to be activated, closely following the variation of the normal conductivity.⁹ Since the conductivity drops exponentially with decreasing temperature, the relaxation process associated with ω_m slows down rapidly. At low temperatures the same phenomenon may appear as weak relaxation of metastable CDW configurations, a process taking place on the time scale of hours. In fact, the stretched exponential polarization decay,

$$P(T) = P_0 \exp \left[- \left(\frac{t}{\tau_n} \right)^{1-n} \right], \quad (4)$$

observed experimentally⁵ in the temperature range of 25–65 K, is closely related to the generalized Debye formula applied in the (65–100)-K interval.⁹ First the characteristic time of this function, τ_n , is also activated and follows the temperature dependence of the normal resistivity.⁵ The exponent in the time dependence,

$1-n=0.7$, has the same value as $(1-\alpha)\beta$ in Eq. (3). More importantly, we found that the appropriate half-Fourier transformation of Eq. (4),

$$\epsilon(\omega) = \epsilon_\infty + \int p'(t) \exp(i\omega t) dt, \quad (5)$$

corresponds to a dielectric function very close to that of Eq. (3) if

$$\tau_n = \tau_m \quad \text{and} \quad 1-n = (1-\alpha)\beta. \quad (6)$$

[Here $p'(t)$ is the time derivative of the polarizability, i.e., the density of charging current following an electric field step of unity]. To show the equivalence of the stretched-exponential relaxation and the generalized Debye formula, we have indicated by solid lines the dielectric response corresponding to Eq. (4) in Figs. 2 and 5. They show good agreement within the experimental accuracy. With this fit our aim is not to give a somewhat different phenomenological description of the low-frequency conductivity, but rather to show that the response in the MHz range at 77 K is the same excitation of the condensate as that which appears in glassy behavior on long-time scales below 30 K.¹⁵

The temperature dependence of τ_m , which follows the variation of the normal conductivity, demonstrates that this relaxation time is governed by screening effects provided by thermally excited electrons. The relevant low-frequency (LF) screening time is given by $\tau_{\text{LF}} = \epsilon_0 \rho_{\text{dc}}$, where ϵ_0 is the background dielectric constant and ρ_{dc} is the dc resistivity. Such screening effects become important when the response of the collective mode involves the gradual buildup of internal deformation, which have to be screened by the uncondensed electrons before further polarization can develop.

Alternatively,^{16,17} the resonances, appearing at the radio-frequency wave spectral range can be described by a relaxation process, between the condensed phonons and the lattice. This relaxation process is characterized by a

relaxation time τ^* , and it determines the low-frequency ac response, which is due to the dynamics of the internal deformations of the collective mode. A frequency-dependent conductivity follows from the quantum-mechanical description of the transition between the various pinned CDW configurations, and it is given by

$$\sigma(\omega) = \exp(-\omega_s / \omega) \quad (7)$$

with $\omega_s = \tau_0^{-1}$ and τ_0 defined as the phenomenological time constant, which incorporates screening by the normal electrons.¹⁸ Equation (7) describes only qualitatively our findings in the radio-frequency spectral range, and we believe that the appropriate description of $\sigma(\omega)$ is in terms of the relaxational dynamics, as in many other localized or glassy systems.

B. Resonances in the millimeter-wave and FIR spectral range: Pinned and bound mode resonances

At frequencies that span the spectral range well below where conventional optical methods lead to reliable results, we have combined a variety of techniques to evaluate the components of the optical conductivity.

The low-frequency dielectric constant, evaluated at audio frequencies using a standard bridge configuration measurement of the sample capacitance, leads to the out-of-phase component σ_2 of the optical conductivity $\sigma = \sigma_1 + i\sigma_2$, through the relation $\epsilon_1 - 1 = 4\pi\sigma_2/\omega$. The components of the optical conductivity was measured directly up to frequencies 5 cm^{-1} by using microwave and millimeter-wave bridge configurations.⁶ σ_1 and σ_2 can be extracted from the measured phase shift ϕ , attenuation A , and the geometrical factors characterizing the specimen dimensions. These values for σ_1 and σ_2 have been used to evaluate the reflectivity R , using the expression

$$R = \frac{1 + (4\pi/\omega)(\sigma_1^2 + \sigma_2^2)^{1/2} - 2\{(2\pi/\omega)[(\sigma_1^2 + \sigma_2^2)^{1/2} - \sigma_2]\}^{1/2}}{1 + (4\pi/\omega)(\sigma_1^2 + \sigma_2^2)^{1/2} + 2\{(2\pi/\omega)[(\sigma_1^2 + \sigma_2^2)^{1/2} - \sigma_2]\}^{1/2}}, \quad (8)$$

where ϵ_∞ (i.e., $\omega \rightarrow \infty$ dielectric constant) has been neglected, since, as will be discussed later, ϵ_∞ is significantly small (i.e., $\approx 10^2$) in comparison to the actual value of $\epsilon_1(\omega)$ (i.e., $\approx 10^4$) in the GHz frequency range.

The reflectivity, from the radio-frequency, microwave, and millimeter wave to the FIR energy spectral range, of $\text{K}_{0.3}\text{MoO}_3$ is displayed in Fig. 6(a) [see also Fig. 3 for the complete $R(\omega)$ spectrum]. The full dots represent the reflectivity values evaluated in the microwave and millimeter-wave spectral range using Eq. (8). The dashed line, at frequencies below 14 cm^{-1} , has been obtained by describing the microwave and millimeter-wave results in terms of two harmonic oscillators (see below). The calcu-

lated $R(\omega)$ within the harmonic oscillators approach agrees perfectly with the reflectivity data as directly evaluated [Eq. (8)] from the microwave and millimeter-wave experiments [see dots in Fig. 6(a)]. Our reflectivity results for $\text{K}_{0.3}\text{MoO}_3$ are in good agreement with the earlier results by Travaglini and Wachter¹⁹ and by Ng, Thomas, and Schneemeyer.²⁰ For example, the shape of the giant absorption below 60 cm^{-1} in our $R(\omega)$ is qualitatively similar to the experimental results of Refs. 19 and 20. However, Ng, Thomas, and Schneemeyer²⁰ reported reflectance data in the FIR, which are about 3% lower than those of Travaglini *et al.*¹⁹ This may come from different surface conditions on the samples measured.

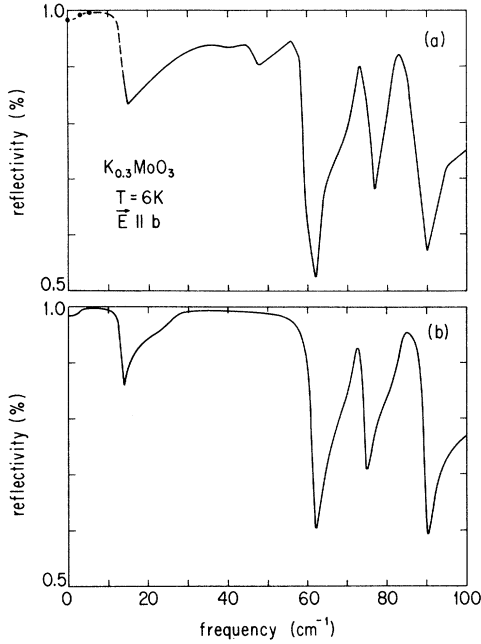


FIG. 6. (a) Reflectivity R vs frequency in the radio-to-infrared spectral range for $K_{0.3}MoO_3$. Dots are the microwave and millimeter-wave data using Eq. (8). The dashed line represents the reconstructed reflectivity within the harmonic oscillator approach (see text). (b) Calculated reflectivity for four harmonic oscillators. The parameters used to calculate $R(\omega)$ are given in the text.

Nevertheless, the absolute value of our $R(\omega)$ was in both cases (i.e., pure and doped compounds) within the range of the experimental data of Refs. 19 and 20. The experimental $R(\omega)$ spectrum was then normalized to the microwave and millimeter-wave data by multiplying the observed reflectance with a factor of 1.01. The dielectric constant and optical experiments were conducted at 6 K; the millimeter-wave data were taken at $T=20$ K. No temperature dependence was observed at these temperatures, and consequently the spectrum can be regarded as the $T \rightarrow 0$ limit of the optical response. The resonances that appear in the 60–100 cm^{-1} spectral range are phonon lines,¹⁹ which can be modeled by a harmonic oscillator description. Below 60 cm^{-1} the features observed are associated with the dynamics of the pinned mode. The reflectivity R is different from 100% as $\omega \rightarrow 0$, rises to a maximum in the millimeter-wave spectral range, followed by a local minimum at higher frequencies. This behavior is characteristic of two resonances in the covered spectral range (i.e., between dc and 60 cm^{-1}). In order to demonstrate this, we have calculated R by assuming that σ is composed of two oscillators with different parameters, i.e.,

$$\begin{aligned} \sigma &= \sigma_{osc1} + \sigma_{osc2} - i \frac{\omega}{4\pi} \epsilon_{\infty} \\ &= \frac{\omega_{p1}^2}{4\pi} \frac{i\omega}{\omega^2 - \omega_{01}^2 + i\omega/\tau_1} \\ &\quad + \frac{\omega_{p2}^2}{4\pi} \frac{i\omega}{\omega^2 - \omega_{02}^2 + i\omega/\tau_2} - i \frac{\omega}{4\pi} \epsilon_{\infty}, \end{aligned} \quad (9)$$

where $\omega_{pi}^2/8$ represents the oscillator strength associated with each resonance and ϵ_{∞} is the contribution from optical structures at higher frequencies. Figure 6(b) shows the calculated reflectivity where the parameters $\omega_{0i}, \omega_{pi}^2/\tau_i$ for the first two resonances are 3.3, 834, 0.67 cm^{-1} and 26.7, 1334, 2.67 cm^{-1} , respectively, and $\epsilon_{\infty} = 600$. All the characteristic features of Fig. 6(a) are well reproduced with these parameters. We also note that the shape of $R(\omega)$ between dc and 60 cm^{-1} , can be recovered only if both resonances simultaneously make a contribution to the reflectivity.³ In Fig. 6(b) we have also described the two phonon modes above ω_{02} in terms of harmonic oscillator (with 71.7 and 83.4 cm^{-1} for the frequencies, 333.6 and 500 cm^{-1} for the mode strengths, and 1.33 and 1.67 cm^{-1} for the dampings, respectively). Moreover, it is interesting to note that with only the parameters of the first harmonic oscillator, describing the collective mode of the CDW, we can also fit the static dielectric constant fairly well [i.e., $\epsilon_1(\omega \rightarrow 0) = \epsilon_{\infty} + (\omega_{p1}/\omega_{01})^2 = 7 \times 10^4$].

For the alloy $K_{0.3}Mo_{0.985}W_{0.015}O_3$ we applied the same procedure and the same set of parameters, except for the frequency of the pinned mode, which was shifted to 10 cm^{-1} , to reconstruct the $R(\omega)$ spectrum. The smaller value of $\epsilon_1(\omega \rightarrow 0) = 7 \times 10^3$, observed directly at low frequencies and due to the shift of the pinned mode to higher frequency, is also recovered within our phenomenological approach.

The reflectivity evaluated over a broad energy spectral range [Figs. 3 and 6(a)] has also been used for the Kramers-Kronig transformation, from which we obtain the optical functions [$\epsilon(\omega)$ and $\sigma(\omega)$]. Figure 7 displays the real part of the dielectric function [$\epsilon_1(\omega)$], where the millimeter and microwave data are also included. $\epsilon_1(\omega)$ is clearly dominated by the huge resonance at ω_{01} . Figures 8 and 9(a) show the optical conductivity [$\sigma_1(\omega)$]. For the sake of clarity, in Fig. 8, we only present $\sigma_1(\omega)$ close to the single-particle gap excitation marked by the

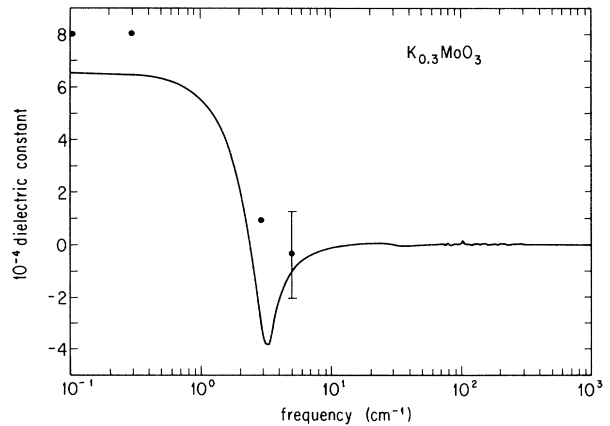


FIG. 7. Dielectric constant for $K_{0.3}MoO_3$ as obtained from the Kramers-Kronig analysis. The full points are ϵ_1 values evaluated directly from the microwave and millimeter-wave experiments for the pure compound.

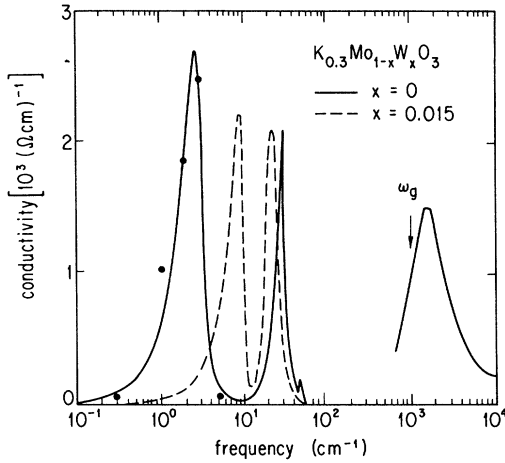


FIG. 8. Experimental optical conductivity for $K_{0.3}Mo_{1-x}W_xO_3$ ($x=0$ and 0.015) as evaluated from the Kramers-Kronig analysis. The arrow represents the single-particle gap as obtained from the dc resistivity. The full points are the σ_1 values obtained directly from the microwave and millimeter-wave experiments in the case of the pure compound.

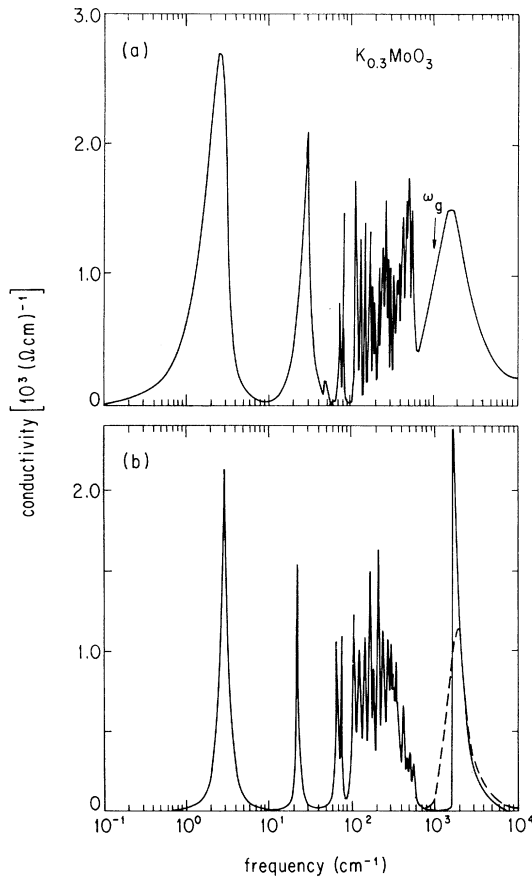


FIG. 9. (a) Complete experimental optical conductivity for $K_{0.3}MoO_3$ as evaluated from the Kramers-Kronig analysis. ω_g represents the single-particle gap obtained from the dc resistivity in the CDW state. (b) Optical conductivity calculated using the model of Ref. 34. The dashed line represents the Gaussian convolution of the single-particle gap.

arrow at ω_g and in the low-frequency range. The spectral range between 100 and 1000 cm^{-1} will be discussed later. The two low-frequency modes are also clearly recovered both for the nominally pure compound and for the alloys. While the low-frequency mode [at 3.33 cm^{-1} (100 GHz) for the pure compound] moves to higher frequencies upon doping, the position of the higher-frequency mode is only slightly modified.

In Fig. 9(a) we present the complete-frequency-dependent response $\sigma_1(\omega)$ for pure $K_{0.3}MoO_3$. Besides the features discussed before, $\sigma_1(\omega)$ is also characterized by numerous sharp structures in the far-infrared spectral range.

The resonance at ω_{01} , the so-called pinning frequency, occurs at 3.33 cm^{-1} for $K_{0.3}MoO_3$ and is due to the oscillatory response of the collective mode.³ Several observations support this assumption. First, our experiments on doped specimens clearly demonstrate the shift of the resonance frequency with increased doping, as expected for a charge-density wave, which is pinned by impurities. Secondly, the effective mass m^* associated with this resonance can be evaluated from the measured oscillator strength

$$\int \sigma_1(\omega) d\omega = \frac{ne^2}{m^*} \frac{\pi}{2} \quad (10)$$

of the resonance. One obtains an effective mass $m^*/m_b = 400$ for $K_{0.3}MoO_3$, in agreement with the analysis based on Eq. (1) and given earlier. This value is in excellent agreement with the mean-field result.²¹ Within the same framework, Pouget also suggests a range for m^*/m_b between 200 and 450 , obtained from the measurements of the amplitude mode with neutron-scattering experiments.²² Using equation (10) on the alloyed materials we found a value of $m^*/m_b = 400$, which is essentially unchanged.

The characteristic relaxation time $1/\tau_{HF}$ of this high-frequency mode (ω_{01}) is 50 GHz around $T=77\text{ K}$ and τ_{HF} progressively increases as the temperature is lowered. The relaxation process is probably mainly due to the interaction of the collective mode with phonon or phason excitations, and some of the relevant processes have been examined theoretically.²³ Introducing random pinning leads to a broadened resonance, but not to the complex response given in Fig. 2.

The resonance that occurs at $\omega_{02} = 40\text{ cm}^{-1}$ in $K_{0.3}MoO_3$ has not yet been explained.³ Below we list some possibilities, but we argue that none of these can be clearly ascribed to the resonance we have observed.

(i) The amplitude mode is Raman active,²¹ but not infrared active in specimens without lattice imperfections which break the translational symmetry. Impurities, which pin the collective mode, could, however, lead to a finite polarization accompanying the amplitude fluctuations. Such a mechanism would then lead to an optical resonance at the amplitude mode frequency ω_A . This frequency has been measured at $\omega_A = 60\text{ cm}^{-1}$ in $K_{0.3}MoO_3$.²⁴ The frequency ω_A is significantly higher than the frequency of the optical resonances. Therefore, we consider this mechanism unlikely.

(ii) It has also been suggested²⁵ that the resonance at ω_{02} in the related compound $(\text{TaSe}_4)_2\text{I}$ (for which $\omega_{01}=1.5 \text{ cm}^{-1}$, $\omega_{02}=38 \text{ cm}^{-1}$, $\omega_A=90 \text{ cm}^{-1}$, and $m^*/m_b=10^4$) is due to an optical phason, which arises due to a periodicity $\tilde{\lambda}=\pi/k_F$ leading to a $q=2k_F$ optically active mode. The relevant frequency is

$$\omega_{\text{op}} \simeq \left[\frac{m_b}{m^*} \right]^{1/2} (v_F q) = \left[\frac{1}{m_b m^*} \right]^{1/2} \frac{4\pi\hbar}{\tilde{\lambda}^2}, \quad (11)$$

where $\tilde{\lambda}$ is the period of the CDW [$\tilde{\lambda}=14 \text{ \AA}$ for $\text{K}_{0.3}\text{MoO}_3$ and 16 \AA for $(\text{TaSe}_4)_2\text{I}$ (Ref. 1)]. As the effective mass of $\text{K}_{0.3}\text{MoO}_3$ is widely different from that of $(\text{TaSe}_4)_2\text{I}$, ω_{op} is expected to differ by approximately a factor of $(10^4/300)^{1/2} \sim 6$ in the two compounds, in clear disagreement with the experimental observations. A similar ratio is expected for the second harmonic phason picture advanced by Walker.²⁶

(iii) At low temperatures, where screening by normal electrons is absent and Coulomb effects are important, the phason dispersion relation develops a gap,²⁷ and at $q=0$

$$\begin{aligned} \omega_{\text{LO}} &= \frac{\omega_{\text{pt}}}{\epsilon_{\Delta}^{1/2}} = \left[\frac{4\pi n e^2}{m^* \epsilon_{\Delta}} \right]^{1/2} \\ &= \frac{\sqrt{6}\Delta}{\hbar} \left[\frac{m_b}{m^*} \right]^{1/2} = (3/2)^{1/2} \omega_A. \end{aligned} \quad (12)$$

In other words, inclusion of Coulomb interaction leads to a long-wavelength phase mode spectrum consisting of an acoustical and an optical branch. It is not clear if the mode from the optical branch should be FIR and/or Raman active. However, the optical-mode frequency is expected to be even higher than the amplitude mode one (ω_A), and, like point (i), we consider this possibility extremely unlikely.

(iv) For charge-density waves near to commensurability, i.e., $\tilde{\lambda}$ close to na with a the lattice parameter, a midgap band inside the main Peierls gap appears due to the so-called soliton lattice.²⁸ Such effects could be important in $\text{K}_{0.3}\text{MoO}_3$, where $\tilde{\lambda}$ is close to $4a$ and commensurability locking has been observed²⁹ in some specimens. However, the resonance frequency associated to these midgap states is nearly one order of magnitude larger than the observed frequencies.

Recently, we proposed an alternative explanation based on a phenomenological Clausius-Mossotti-type model. We suggest that the FIR mode is due to bound collective-mode states, analogous to bound phonon states in semiconductors.³⁰ This approach accounts for both resonances (ω_{01} and ω_{02}) in terms of an effective-medium theory. First of all, the model takes into account an unperturbed dielectricum [$\epsilon_m(\omega)$], which is dominated by the ac response of the pinned collective mode, usually described by a harmonic oscillator. Within the spherical volume around the impurities the dielectric function is then assumed to be the sum of the above harmonic oscillator and a frequency-independent contribution (ϵ_i) due to the impurity itself.^{30,31} The standard approach for a random distribution of such (nonoverlapping) spheres of

dielectric function $\epsilon_s(\omega)$ ($=\epsilon_m(\omega)+\epsilon_i$), immersed in a medium with dielectric function $\epsilon_m(\omega)$, leads to the effective dielectric function of the medium:³⁰

$$\epsilon_{\text{eff}} = \epsilon_m + \frac{3\epsilon_m(\epsilon_s - \epsilon_m)f}{\epsilon_s + 2\epsilon_m - (\epsilon_s - \epsilon_m)f}, \quad (13)$$

where f is the dimensionless filling factor.

The excess polarizability around the defects (essentially described by ϵ_i) leads to a locally modified effective dielectric function which has then two zero crossings: one at ω_{LO} (i.e., the longitudinal frequency of the collective mode) and one at $\omega < \omega_{\text{LO}}$. This situation leads to a new absorption in the excitation spectrum besides the absorption due to the pinned CDW mode. The application of this phenomenological approach to $\text{K}_{0.3}\text{MoO}_3$ reproduces our experimental findings in the energy range from the microwave and millimeter wave up to the FIR frequencies. Indeed, ϵ_{eff} has two resonances at 3.33 and at 40 cm^{-1} , which mimic the two experimental absorptions as clearly found in the reflectivity spectrum [e.g., see Fig. 6(a)].³¹ We made use of a filling factor $f=0.2$. This implies, by a residual impurity concentration N_s of approximately 10^{18} cm^{-3} and using the expression $f = \frac{4}{3}\pi N_s r_s^3$, a characteristic radius r_s around the impurities of about 40 \AA . Within a recent strong pinning theory of CDW dynamics, our r_s is in good agreement with the length scale [$=\xi_{\parallel}(A_0/2\xi_{\perp}^2)^{1/2}$, ξ_{\parallel} represents the CDW amplitude coherence length along the chain direction and ξ_{\perp} in the transverse direction, and A_0 is the cross sectional area] corresponding to a volume surrounding the individual impurities sites, where the adjustment between the average CDW phase and the pinned value takes place.³² The parameters defining the collective-mode resonance [i.e., the harmonic oscillator, which describes $\epsilon_m(\omega)$] have values very close to those used previously for the analysis of the reflectivity spectrum [Fig. 6(b)]. For ϵ_i , however, we estimated a value of 1000. We can justify the ϵ_i value within the usual treatment of impurity states in semiconductors [$\alpha = V(\epsilon_i - 1)/4\pi$, where V is the volume of the spheres], which uses the vacuum polarizability (α) of the H atom ($0.67 \times 10^{-24} \text{ cm}^3$), and the dielectric-constant enhancement $\eta \simeq \epsilon_{\infty}^4$ as input parameters (i.e., $\epsilon_{\infty} \simeq 100$).³¹ Such a large impurity-induced dielectric constant is due to impurity-induced resonances below the Peierls gap. Nevertheless, optical experiments in the spectral range somewhat below Δ , while highly suggestive of such resonances, are somehow controversial.³³ A full account of our analysis of this mode will be published elsewhere.³¹

C. Conductivity in the optical spectral range: Single-particle transition and phase phonons

In the infrared-to-visible spectral range a broad resonance, appearing at the frequency where the dc conductivity indicates the appearance of the single-particle gap, and several intense phonon peaks dominate the optical conductivity. Both are clearly associated with the dynamical response of the collective mode, and first we give a short theoretical overview of the effects that are ex-

pected, and then compare these with our experimental findings.

The electrical conductivity and dielectric response of CDW's was earlier investigated by Lee, Rice, and Anderson (LRA).²¹ The starting point of the model is the one-dimensional Fröhlich's Hamiltonian, where the coupling of noninteracting electrons to phonons in a jellium model or in an incommensurate situation is taken into account and where a particular emphasis is given to the role played by the collective mode. The total optical conductivity is given by²¹

$$\sigma(\omega) = \frac{\omega_p^2}{4\pi\omega i} \left[\frac{f(\omega)}{1 + (\lambda\omega_Q^2/4\Delta^2)f(\omega)} - f(0) \right], \quad (14a)$$

where

$$f(\omega) = \frac{2\Delta^2}{\omega^2 y} \left[\pi i + \ln \frac{1-y}{1+y} \right], \quad f(0) = 1 \quad (14b)$$

and

$$y = \left[1 - \frac{4\Delta^2}{\omega^2} \right]^{1/2}. \quad (14c)$$

λ is the dimensionless electron-phonon coupling constant, ω_Q is the phonon frequency at $2k_F$ (of the order of 50 K), and 2Δ denotes the energy gap. Within a mean-field approach the dimensionless coupling constant λ is related to the mass enhancement m^*/m_b by the relation:

$$m^*/m_b = 1 + 4\Delta^2/\lambda\omega_Q^2. \quad (15)$$

In the case $m^*/m_b \rightarrow \infty$, $\sigma(\omega)$ has the form appropriate to an insulator, with band-to-band transition and zero dc current. However, with a finite m^*/m_b in the absence of pinning and damping $\sigma(\omega=0) = ne^2/i\omega m^*$. This implies, by the Kramers-Kronig relation, a δ function at $\omega=0$ for $\sigma_1(\omega)$, with relative spectral weight m_b/m^* . This weight is removed from the ac conductivity, and the square-root singularity at $\omega=2\Delta$ given by Eq. (14a) for $m/m^* \rightarrow 0$ becomes a square-root edge (see, e.g., Fig. 2 of Ref. 21).

A slightly different approach was proposed by Rice.³⁴ Again a linear-chain system is considered, where the conduction electrons move in a periodic potential V of wave vector $q_0 = 2k_F$ and are coupled to a set of G distinct phonon bands. (The model does not specify the precise nature of these bands; in general many of them will be associated with those intramolecular vibrations that induce modulation of the local conduction-electron density.) The key point of this model is that in addition to the single-electron contribution, collective contributions associated with oscillations in the phases of the combined lattice and charge distributions about their zero equilibrium values will also be observed. Such oscillations involve a bodily displacement of an appropriate component of the condensed charge and are therefore optically active along the chain direction. The situation closely parallels that found by Lee, Rice, and Anderson for the collective mode of an acoustic-phonon-stabilized Fröhlich CDW state.²¹ The frequency-dependent conductivity $\sigma(\omega)$

along the chain direction is given by

$$\sigma(\omega) = \frac{\omega_p^2}{4\pi i \omega} \left[f \left[\frac{\omega}{2\Delta} \right] - f(0) - \left[\frac{\omega}{2\Delta} \right]^2 f \left[\frac{\omega}{2\Delta} \right]^2 \lambda' D_\phi(\omega) \right], \quad (16a)$$

where

$$D_\phi(\omega)^{-1} = D_0(\omega)^{-1} + 1 - \frac{V}{\Delta} + \frac{\lambda'\omega^2}{4\Delta^2} f \left[\frac{\omega}{2\Delta} \right] \quad (16b)$$

and

$$D_0(\omega) = - \sum_{n=1}^G \frac{\lambda_n}{\lambda'} \frac{\omega_n^2(q_0)}{\omega_n^2(q_0) - \omega^2 - i\omega\Gamma_n}. \quad (16c)$$

$f(\omega)$ is given by Eq. (14b), ω_p is the (unscreened) plasma frequency of the noninteracting electrons, $\lambda' = \sum_n \lambda_n$ and λ_n are the dimensionless electron-phonon coupling constant conventionally defined to characterize the strength of the conduction-electron coupling to the n th phonon band [i.e., $\lambda_n = N(0)g_n^2/\omega_n(q_0)$, where $N(0)$ is the density of states at the Fermi level and g_n the linear coupling constant specifying the interaction of the conduction electron with the n th phonon band]. ω_n and Γ_n are the frequencies and the dampings of the bare phonons, which are coupled to the electronic density fluctuation of wave vector q . λ' , ω_p , 2Δ , and V are related to the static dielectric constant ϵ_0 through the formula

$$\epsilon_0 = 1 + \left[\frac{\omega_p}{2\Delta} \right]^2 \left[\frac{2}{3} + \frac{\lambda'\Delta}{V} \right]. \quad (17)$$

The first two terms in Eq. (16a) describe the usual electron transitions across the semiconducting energy gap 2Δ . The third term, which contains the so-called phononlike propagator $D_\phi(\omega)$, describes the additional optical activity arising from the phase phonons. These phonons are indeed the zeros of $D_\phi(\omega)$ [Eq. (16b)], and each of them takes out spectral weight from the single-particle gap. This is true only for $\omega < 2\Delta$, while for $\omega > 2\Delta$ the phonons correspond to the zeros of $D_0^{-1}(\omega) + 1 - V/\Delta$ and appear as "indentations" in the single-particle absorption envelope (Fano-like resonances).

We applied both theoretical approaches, to account for the measured optical conductivity,¹⁰ and Fig. 9(b) shows the result of our calculation using the model of Rice. The calculation was performed by taking into account both the pinned mode at ω_{01} and the FIR resonance at ω_{02} , in addition to the "phonon modes" between 40 and 700 cm^{-1} (see below). The parameters used for the calculation are summarized in Table I. There is a fair agreement with Fig. 9(a) and the essential features of the experimental optical conductivity are well reproduced.

We also point out that 2Δ , ω_p , ϵ_0 , and the frequencies ω_n were directly extracted from the experimental results, and the parameters Γ_n of the FIR absorptions were slightly adjusted in order to obtain the best simulation of the experimentally found $\sigma_1(\omega)$. The frequencies ω_n

TABLE I. Parameters used for the calculation of $\sigma_1(\omega)$ using the model of Ref. 34; unscreened plasma frequency ω_p , gap Δ , dielectric constant ϵ_0 , and the bare mode's frequencies (ω_n) dampings (Γ_n), and electron-phonon coupling constants (g_n): $\omega_p=2.7$ eV (21 777 cm^{-1}), $\Delta=0.1$ eV (807 cm^{-1}), $\epsilon_0=7 \times 10^4$.

ω_n (cm^{-1})	Γ_n (cm^{-1})	g_n (cm^{-1})	ω_n	Γ_n	g_n
10	0.5	201	285	20	479
30	2	348	310	20	500
70	6	238	330	20	516
80	2	254	355	20	536
112	10	301	370	20	546
130	10	323	380	20	553
150	10	348	395	20	564
175	10	376	430	20	589
190	10	391	445	20	599
220	10	422	475	30	619
245	20	444	515	30	644
255	20	454	570	40	678

were fixed in general by the resonances in the absorption spectrum (ϵ_2) obtained by the Kramers-Kronig (KK) analysis. However, in order to reproduce the pinned-mode resonance experimentally observed at 3 cm^{-1} , we were forced to set the corresponding-mode frequency equal to 10 cm^{-1} in our application of the Rice model. For the sake of simplicity, we set the mode strengths λ_n for the first two resonances equal, and this applies also to the case of the bare phonons. Furthermore, transforming our λ_n in the linear coupling constant g_n [where $N(0)=2$ ($\text{eV spin})^{-1}$ (Ref. 19)] we obtain values between 25 and 84 meV (Table I), which are consistent with previous calculations.³⁵ With this choice of the input parameters we obtain, using Eq. (17), the ratio $V/\Delta=0.01$. We note that V/Δ is strongly influenced by ϵ_0 , which we chose to be consistent with our KK transformation. However, from the experimental point of view ϵ_0 can vary between 10^4 and 10^5 , and this translates to a value of V/Δ between 0.01 and 0.1. The smallness of this parameter indicates that the semiconducting state arises predominantly from the periodic distortion. Values between 0.01 and 0.1 are also found in similar calculation on organic CDW compounds.^{34,35}

Next we discuss the sharp structure, which appears close to 2Δ in Fig. 9(b), and which arises due to the single-particle excitations across the Peierls gap. A similar feature, with a square-root singularity for $m^*/m_b \rightarrow \infty$, is also obtained by the application of the LRA model. Our experiment, in contrast, shows a broad structure, in spite of the large effective mass $m^*/m_b=300$. We believe this is a signature of a gap distribution reflecting anisotropy effects. We modeled this distribution by convoluting the theoretical curve obtained for the LRA and Rice models, with a Gaussian distribution of 0.04 eV (323 cm^{-1}) width. The resulting dashed line qualitatively reproduces the rounded shape of the experimentally found single-particle excitation.

As discussed earlier, the sharp lines below 2Δ are ascribed to the FIR optical activity enhanced by the electron-phonon coupling (i.e., the so-called phase pho-

sons). The latter interaction, in effect, causes those phonons (which would be inactive without electron-phonon coupling, and which are essentially due to Raman active intramolecular modes), renormalized as collective modes, to become FIR active in the chain direction. We remark also that the phase phonon spectrum is not altered by our Gaussian convolution of the single-particle gap. Contrary to what has been done for the TEA(TCNQ)₂ compound,³⁵ it is difficult to perform a realistic phonon analysis here because of the low symmetry [i.e., monoclinic ($C2/m$)] and of the large number of atoms (20 formula unit) in the primitive cell. Indeed, for TEA(TCNQ)₂ the phase phonons can be mapped onto the corresponding bare Raman active intramolecular modes, an identification that is not possible to perform here. In this regard, our application of the phason model is comparable to that of Challener and Richards for the NbSe₃ compound³⁶ and to the phenomenological approach, in terms of a factorized dielectric function, on Rb_{0.3}MoO₃ by Jandl *et al.*³⁷

Within the framework of the description discussed above, the lowest-frequency phase mode of this multiphonon stabilized Fröhlich CDW state should correspond to bulk oscillation in the phase of the order parameter Δ , and then it would be identical to the Fröhlich mode of the single-phonon coupling model.^{21,34} Nevertheless, the oscillator strength of the pinned collective mode was included in our application of the Rice model by treating it as a low-frequency phonon mode.³⁶ The spectral weight associated to the latter resonance evaluated from the fit to the experimental found $\sigma(\omega)$ corresponds to value of m^*/m_b of about 400, which is in good agreement with our experimental result and with the previous estimation. We also note, that the FIR model (ω_{02}) was included in our calculation by describing it as a resonance at 30 cm^{-1} in the phononlike propagator $D_\phi(\omega)$. However, an identification of this latter resonance is beyond the purpose of the phase-phonon model, and other approaches, discussed earlier, have to be invoked in order to clarify its origin.^{30,31}

D. Relation to the dielectric-field-dependent conductivity

The two lower-frequency resonances (appearing at the radio frequency and millimeter-wave-frequency range) are also clearly related to the electric-field-dependent response. In general the dielectric constant $\epsilon_1(\omega \rightarrow 0)$ is related to the threshold field for the onset of nonlinear conduction through the relation^{38,39}

$$\epsilon_1(\omega \rightarrow 0)E_T = Ae \quad (18)$$

with A a numerical constant of the order of 1. The low-frequency response, due to the dynamics of internal deformations leads to a large $\epsilon_1(\omega \rightarrow 0)$ and consequently to a small threshold field E_T^* as observed. At $T=77$ K for example [see the corresponding $\sigma_1(\omega)$ in Fig. 2] $\epsilon_1(\omega \rightarrow 0) = 1.1 \times 10^7$ and the threshold field $E_T^* = 200$ mV/cm. These two values lead to $A=0.44$ in good agreement with the values observed on other materials with a CDW ground state.² The dielectric constant ϵ_1 due to the pinned mode is given by

$$\epsilon_1(\omega=0) = 1 + 4\pi n e^2 / m^* \omega_0^2 \quad (19)$$

giving with $\omega_0 = 100$ GHz and $n = 5.4 \times 10^{21}$ cm⁻³ to $\epsilon_1(\omega=0) = 10^5$ in agreement with the direct measurement of the low-frequency dielectric constant.² The experimentally found threshold field $E_T = 10$ V/cm then leads to $A=0.2$, a value again close to unity.

IV. CONCLUSION

We have examined the various excitations of the charge-density-wave state of the model compound $K_{0.3}MoO_3$. In the radio-frequency spectral range, $\sigma(\omega)$ is

determined by the dynamics of internal deformations of the collective mode, which are also strongly influenced by normal electron screening. Consequently, this response is strongly temperature dependent. At millimeter-wave frequencies, the response of the pinned mode, which executes an oscillating motion in response to the applied ac fields, is observed. A far-infrared resonance is identified as due to bound charge-density-wave states, which develop around impurities. The large oscillator strength associated with phonon modes in the CDW state is ascribed to the phase-phonon coupling. We also observe the single-particle gap and discuss the spectral features of the single-particle excitations.

All the above features can be described by various parameters such as effective mass, pinning frequency, electron-phonon coupling constants and relaxation times. These have been compared with values arrived at by various models of charge density wave dynamics.

Finally, we do not find any conclusive evidence for a midgap state at 600 cm⁻¹, and the reflectivity spectrum does not change upon doping.

ACKNOWLEDGMENTS

We wish to thank John Bardeen, M. J. Rice, K. Holczer, P. Littlewood, and A. Virosztek for useful discussions. We wish also to thank S. Donovan, Y. M. Kim, and T. W. Kim for their help and experimental effort during the first stage of the research. One of us (L.D.) wishes to acknowledge P. Wachter for many valuable discussions and the financial support of the Swiss National Science Foundation. This research was supported by the NSF Grant No. DMR 89-13236.

*Permanent address: Central Research Institute of Physics, Budapest, Hungary.

¹For a review see: G. Grüner, *Rev. Mod. Phys.* **60**, 1129 (1988).

²G. Mihály, T. W. Kim, and G. Grüner, *Phys. Rev. B* **39**, 13009 (1989).

³S. Donovan, Y. Kim, B. Alavi, L. Degiorgi, and G. Grüner, *Solid State Commun.* **75**, 721 (1990).

⁴G. Mihály, T. Chen, T. W. Kim, and G. Grüner, *Phys. Rev. B* **38**, 3602 (1988).

⁵G. Kriza and G. Mihály, *Phys. Rev. Lett.* **56**, 2529 (1986).

⁶S. Sridhar, D. Reagor, and G. Grüner, *Rev. Sci. Instrum.* **56**, 1946 (1985); Z. L. Buravov and I. F. Schegolev, *Prib. Tekh. Eksp.* **14**, 171 (1971).

⁷R. P. Hall, M. S. Sherwin, and A. Zettl, *Solid State Commun.* **54**, 683 (1985).

⁸D. Reagor and G. Mozurkewich (unpublished).

⁹R. J. Cava, R. M. Fleming, P. Littlewood, E. A. Rietman, L. F. Schneemeyer, and R. G. Dunn, *Phys. Rev. B* **30**, 3228 (1984).

¹⁰Y. Kim, L. Degiorgi, B. Alavi, and G. Grüner, *Synth. Metals* **41-43**, 3959 (1991).

¹¹G. Mihály, *Synth. Metals* **41-43**, 3799 (1991).

¹²R. M. Fleming, in *Low-Dimensional Conductors and Superconductors*, edited by D. Jérôme and J.-G. Caron (Plenum, New York, 1987), p. 433.

¹³K. V. Ramanujachary, B. T. Collins, M. Greenblatt, R.

Gerhardt, and E. A. Rietman, *Phys. Rev. B* **38**, 7243 (1988).

¹⁴S. Havriliak and S. Negami, *J. Polym. Sci. C* **14**, 99 (1966).

¹⁵P. B. Littlewood and R. Rammal, *Phys. Rev. Lett.* **58**, 524 (1987); *Phys. Rev. B* **38**, 2675 (1988).

¹⁶J. Bardeen, *Physica B&C* **143**, 14 (1986).

¹⁷J. Bardeen, *Phys. Rev. Lett.* **62**, 2985 (1989).

¹⁸J. R. Tucker, W. G. Lyons, J. H. Miller, R. E. Thorne, and J. W. Lyding, *Phys. Rev. B* **34**, 9038 (1987).

¹⁹G. Travaglini and P. Wachter, *Phys. Rev. B* **30**, 1971 (1984).

²⁰H. K. Ng, G. A. Thomas, and L. F. Schneemeyer, *Phys. Rev. B* **33**, 8755 (1986).

²¹P. A. Lee, T. M. Rice, and P. W. Anderson, *Solid State Commun.* **14**, 703 (1974).

²²J. P. Pouget, in *Low-Dimensional Electronic Properties of Molybdenum Bronze and Oxides*, edited by C. Schlenker (Kluwer Academic, Holland, 1989), p. 87.

²³S. Takada, K. Y. M. Wong, and T. Holstein, *Phys. Rev. B* **32**, 4639 (1985); K. Maki and A. Virosztek, *ibid.* **39**, 2511 (1989).

²⁴G. Travaglini, I. Mörke, and P. Wachter, *Solid State Commun.* **45**, 289 (1983).

²⁵M. S. Sherwin, A. Zettl, and P. Richards, *Phys. Rev. B* **36**, 708 (1987).

²⁶M. B. Walker, *Can. J. Phys.* **56**, 127 (1978).

²⁷K. W. Wong and S. Takada, *Phys. Rev. B* **36**, 5476 (1987).

²⁸K. Machida and M. Nakano, *Phys. Rev. Lett.* **55**, 1927 (1985).

- ²⁹J. P. Pouget and R. Comes, in *Modern Problems in Condensed Matter Sciences, Vol. 25*, edited by L. P. Gor'kov and G. Grüner (North-Holland, Amsterdam, 1989).
- ³⁰A. S. Barker, Jr., *Phys. Rev. B* **7**, 2507 (1973).
- ³¹L. Degiorgi and G. Grüner, *Phys. Rev. B* **44**, 7820 (1991).
- ³²W. G. Lyons and J. R. Tucker, *Phys. Rev. B* **38**, 4303 (1988).
- ³³M. E. Itkis and F. Ya. Nad', *Pis'ma Zh. Eksp. Teor. Fiz.* **39**, 373 (1984) [*JETP Lett.* **39**, 448 (1984)]; G. Minton and J. W. Brill, *Synth. Met.* **29**, F481 (1989).
- ³⁴M. J. Rice, *Phys. Rev. Lett.* **37**, 36 (1976); *Solid State Commun.* **25**, 1083 (1978).
- ³⁵M. J. Rice, L. Pietronero, and P. Brüesch, *Solid State Commun.* **21**, 757 (1977).
- ³⁶W. A. Challener and P. L. Richards, *Solid State Commun.* **52**, 117 (1984).
- ³⁷S. Jandl, M. Banville, C. Pépin, J. Marcus, and C. Schlenker, *Phys. Rev. B* **40**, 12 487 (1989).
- ³⁸Wei-yu Wu, A. Janossy, and G. Grüner, *Solid State Commun.* **49**, 1013 (1984).
- ³⁹G. Mihály, T. Chen, and G. Grüner, *Phys. Rev. B* **38**, 12 740 (1988).